

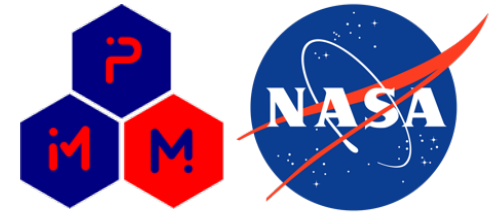
PuMA and Multiscale Modeling

Presenters: Federico Semeraro

Krishnan S. Gopalan

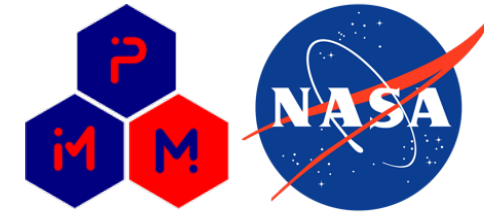
Project contributors: Joseph C. Ferguson, Marcos Acin,
Arnaud Borner, John Thornton
Francesco Panerai, Nagi N. Mansour

Content



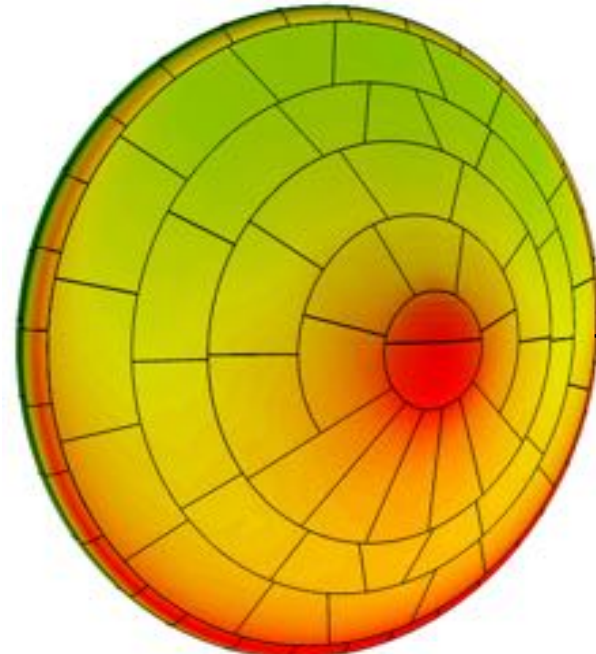
- Motivation
- Overview of PuMA
- Effective properties for fibrous media
 - ❖ Fiber orientation
 - ❖ Thermal conductivity
 - ❖ Elasticity
- Surface chemistry
 - ❖ Molecular beam
 - ❖ Oxidation model

Modeling Thermal Protection Systems



Macroscale Modeling

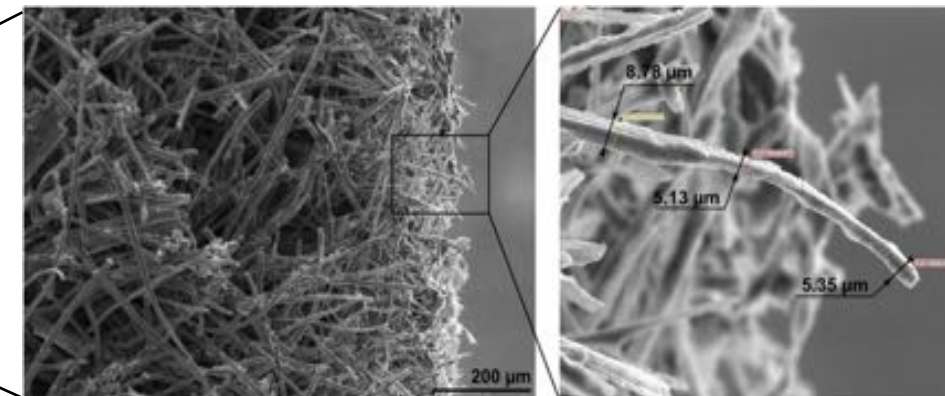
Full scale material response solvers, using volume-averaged techniques to solve conservation equations for ablation



Simulation of surface temperature
for MSL heatshield

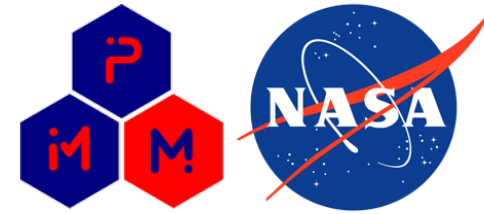
Microscale Modeling

Used to inform material properties and material response parameters used in macro-scale modeling



Lachaud and Mansour, *JTHHT* 2013

X-Ray Microtomography



Collect X-ray images of the sample as you rotate it through 180°

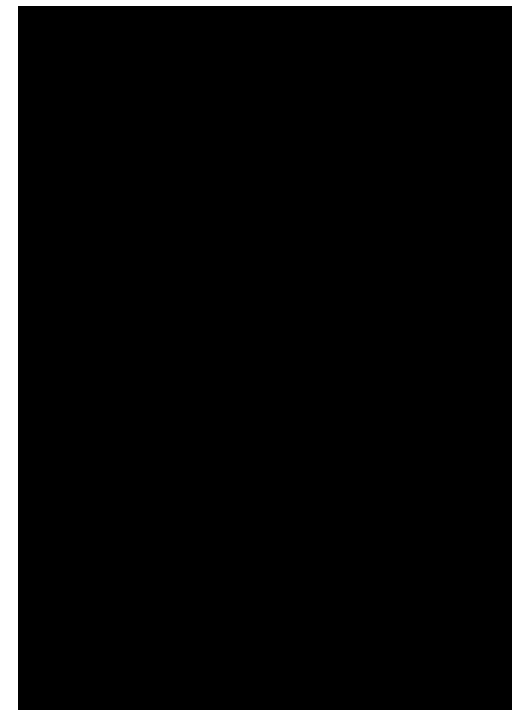


Penetrating power



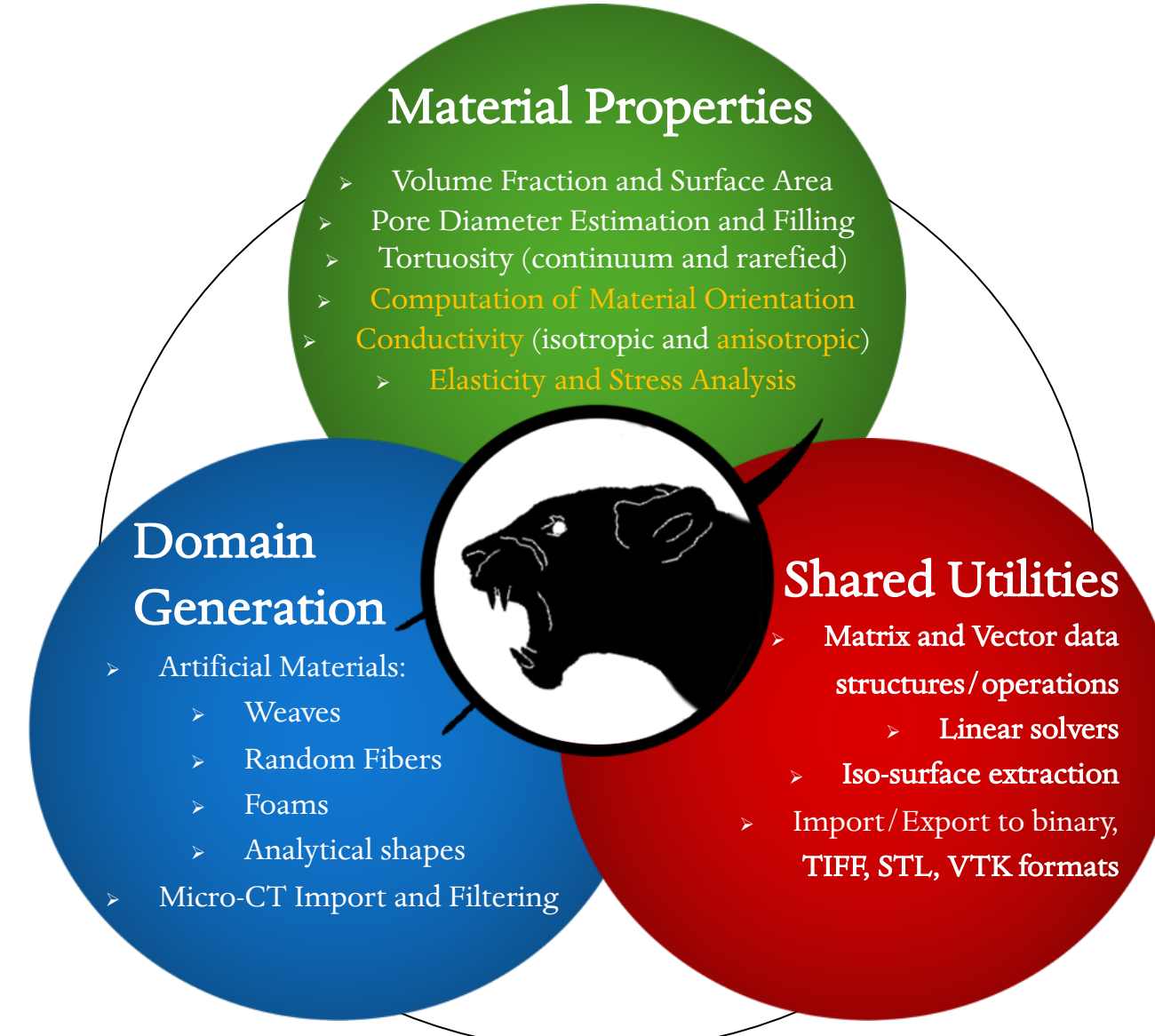
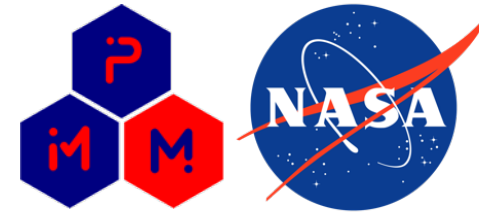
Multiple angles

Use this series of images to reconstruct the 3D object



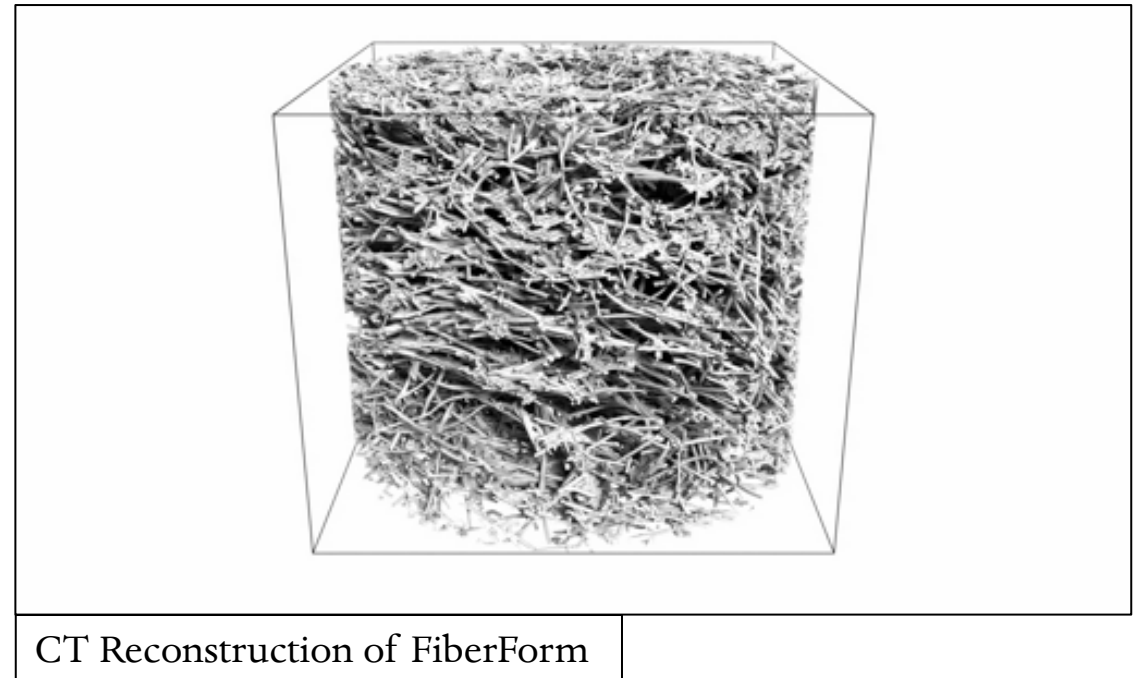
Courtesy of D. Parkinson (ALS)

Porous Microstructure Analysis (PuMA)



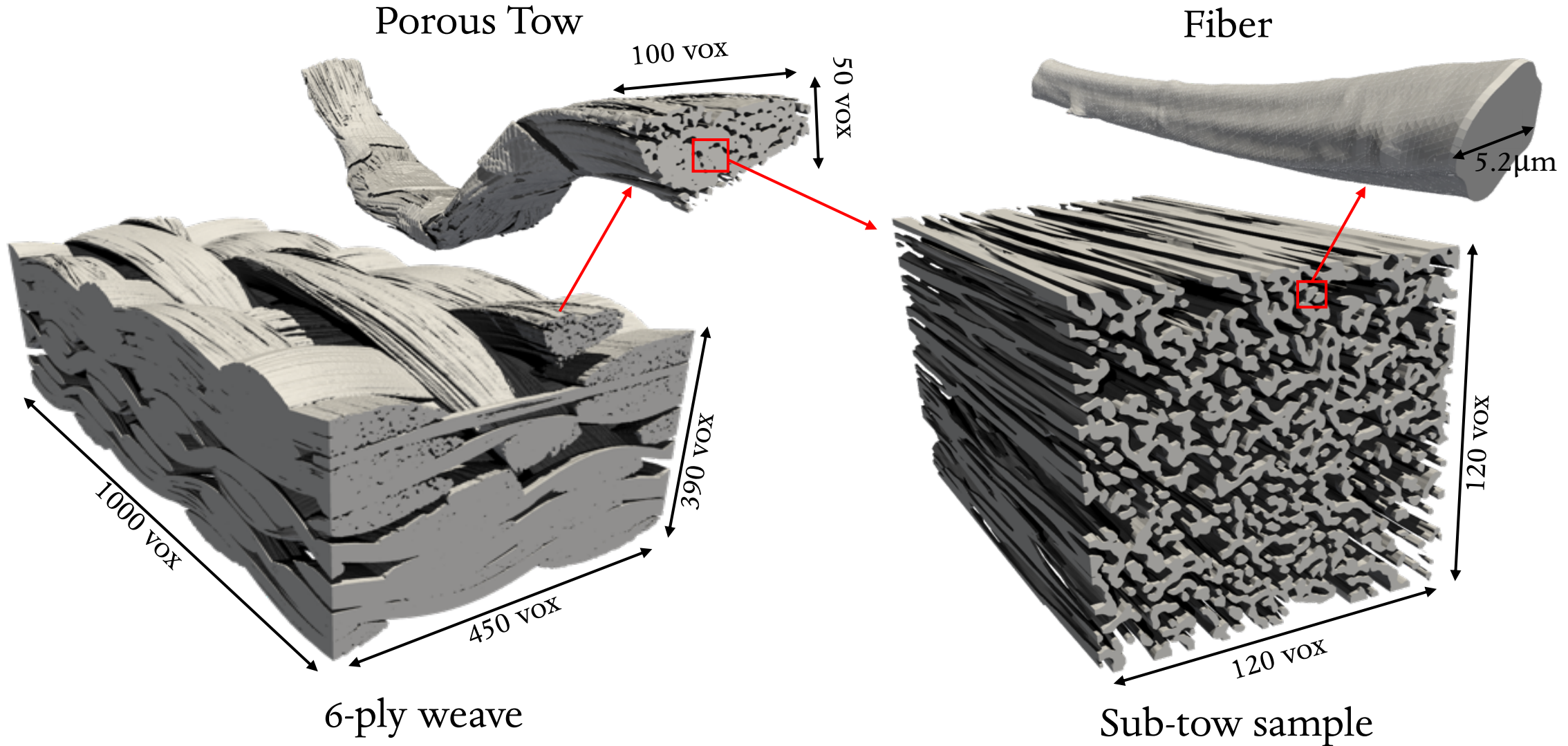
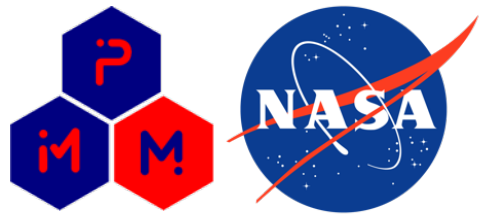
New features in Version 3:

- Modular C++ library
- Redesigned GUI
- Wrapped as Python module
- Linux and Mac compatibility



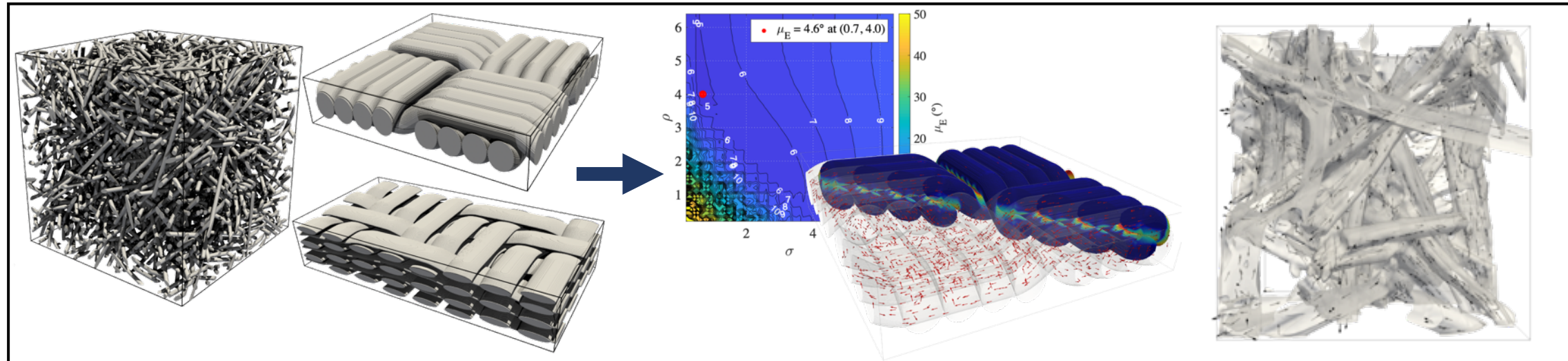
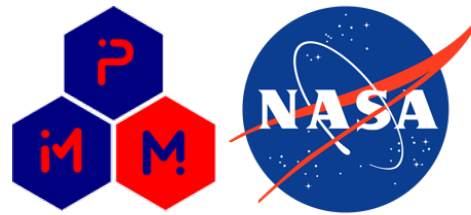
CT Reconstruction of FiberForm

A Multiscale Problem

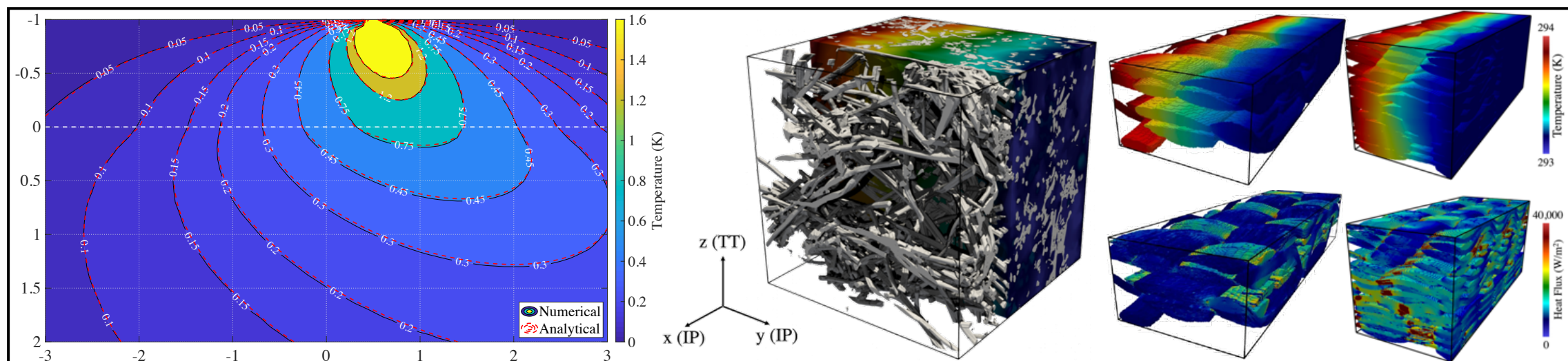


Effective properties for fibrous media

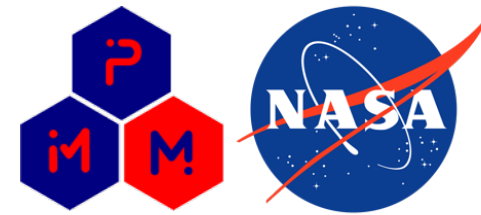
Semeraro, F., Ferguson, J.C., Panerai, F., King, R.J. and Mansour, N.N., Anisotropic analysis of fibrous and woven materials
part 1: Estimation of local orientation. *Computational Materials Science*, 178, p.109631. (2020)



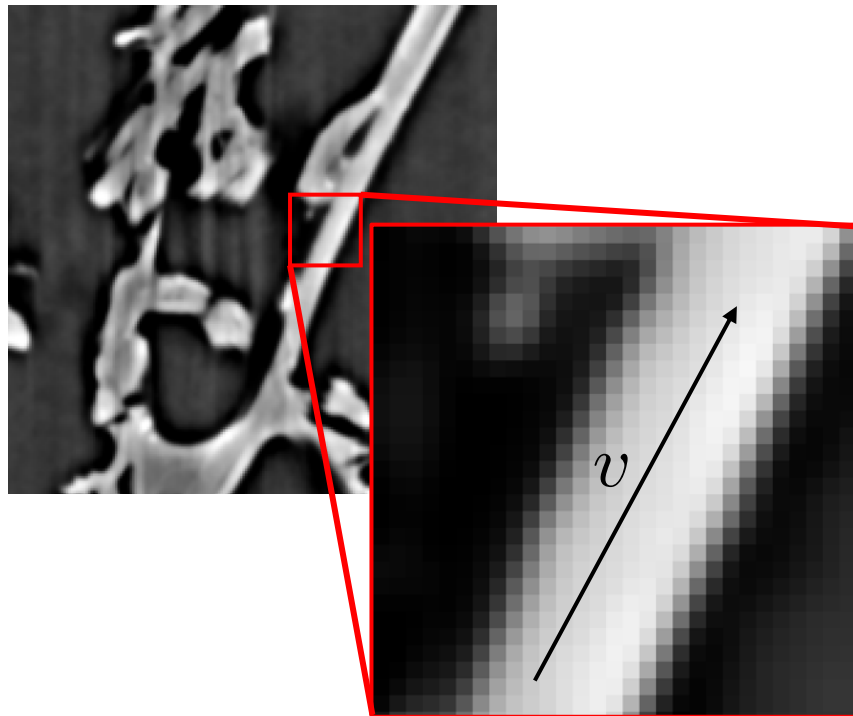
Semeraro, F., Ferguson , J.C, Acin, M., Panerai, F. and Mansour, N.N., Anisotropic analysis of fibrous and woven materials
part 2: Computation of effective conductivity. *Computational Materials Science*, 186, p.109956. (2021)



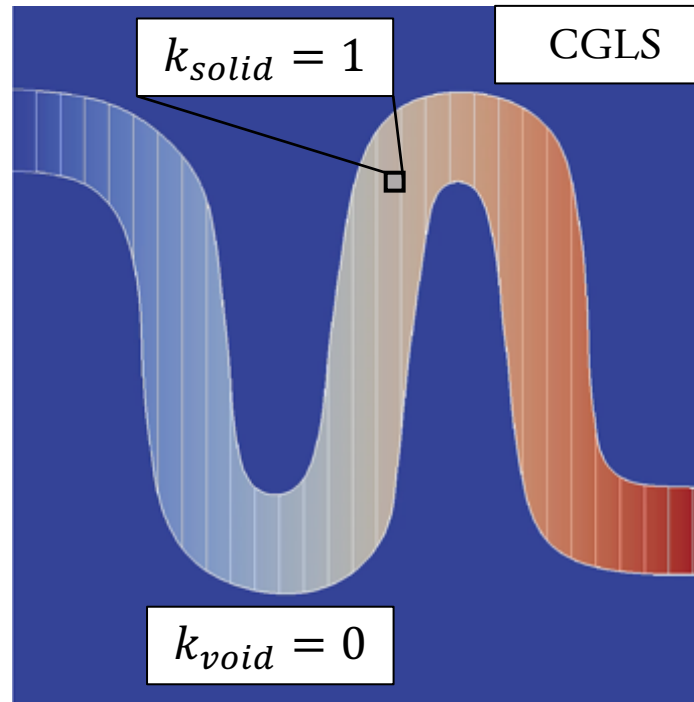
Fiber Orientation Methods



Structure Tensor



Artificial Flux

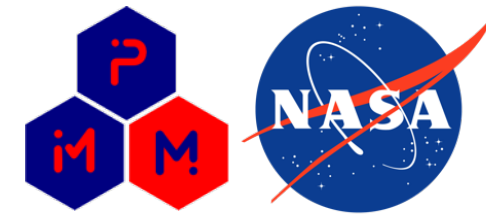


Ray Casting

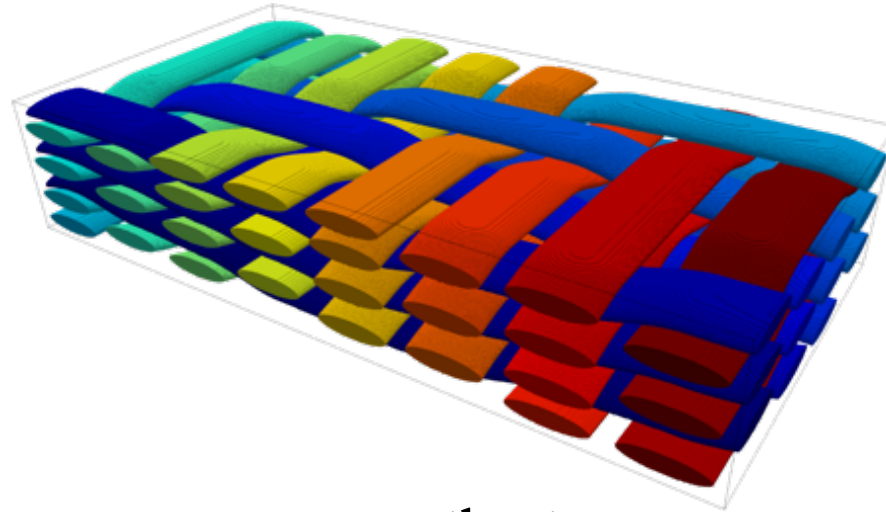


$$(I(x + v) - I(x))^2 \approx 0$$

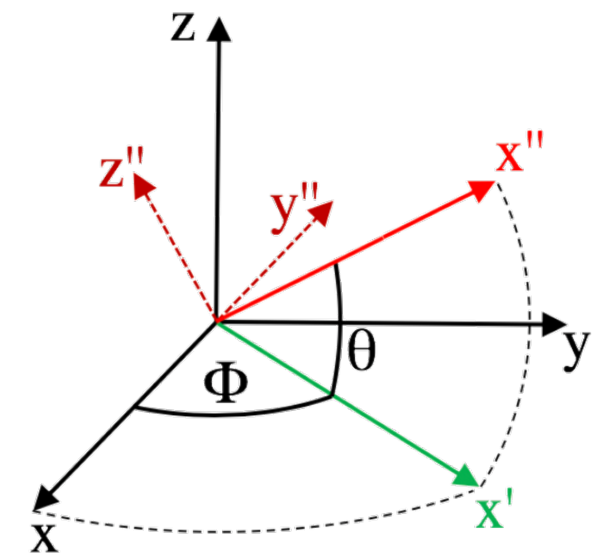
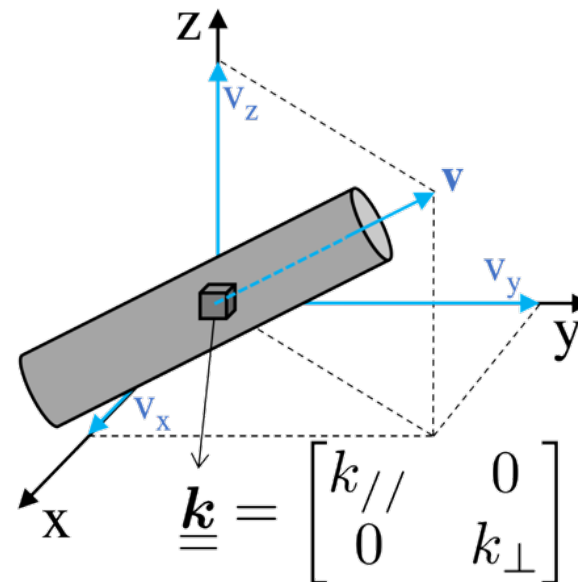
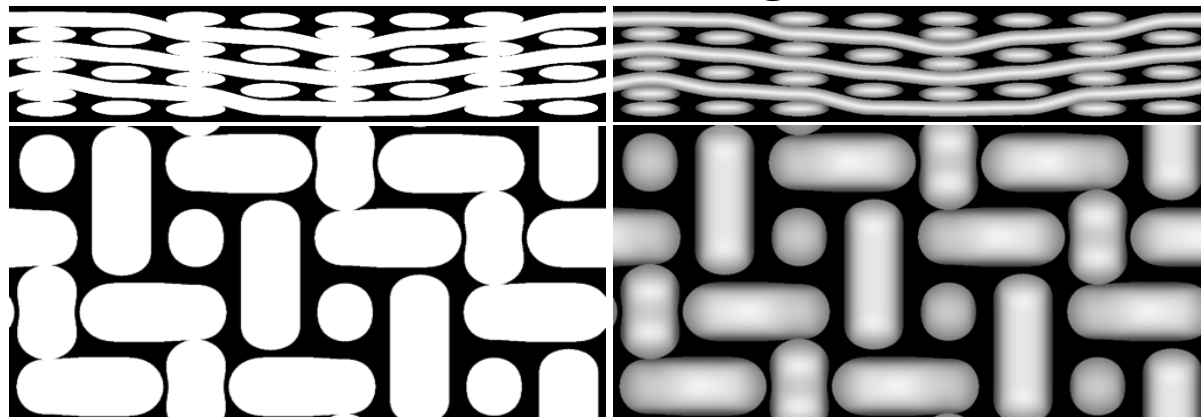
Workflow for Weave Orientation



Individual tow segmentation



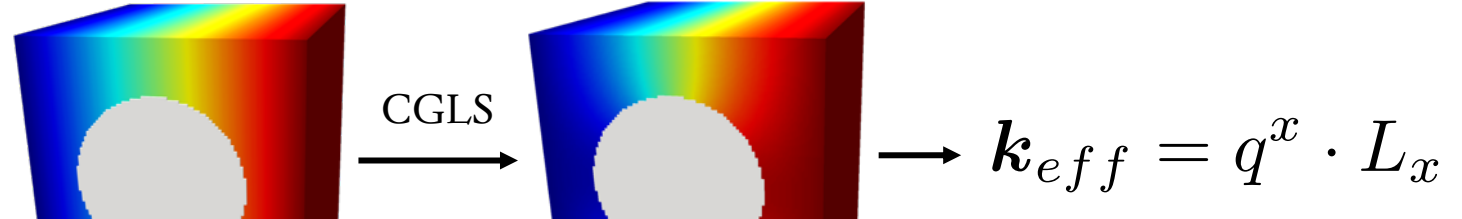
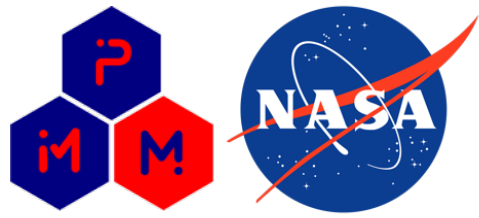
Mean Filtering



$$q = \underbrace{\left[R^{-1} k'' R \right]}_k \nabla T$$

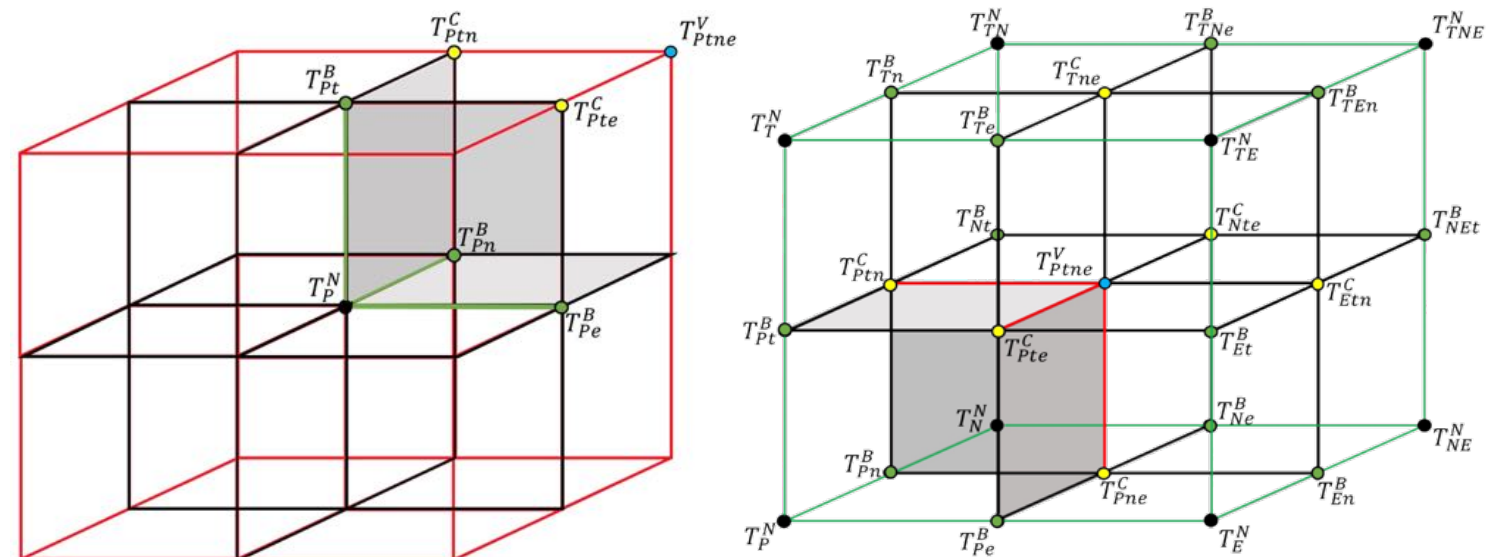
$$R = \begin{bmatrix} \cos \theta & 0 & -\sin \theta \\ 0 & 1 & 0 \\ \sin \theta & 0 & \cos \theta \end{bmatrix} \begin{bmatrix} \cos \phi & \sin \phi & 0 \\ -\sin \phi & \cos \phi & 0 \\ 0 & 0 & 1 \end{bmatrix}^9$$

Effective Thermal Conductivity

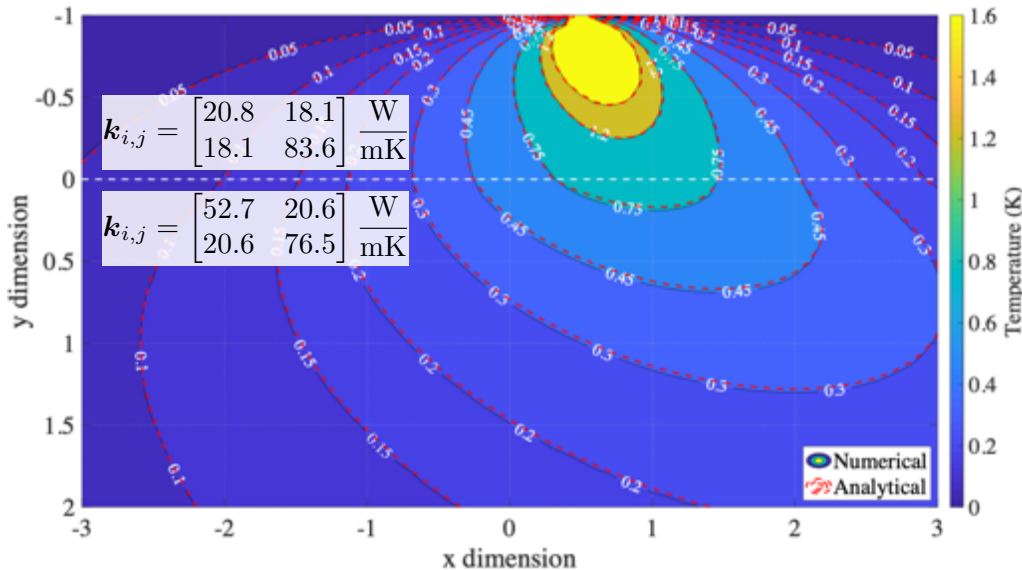
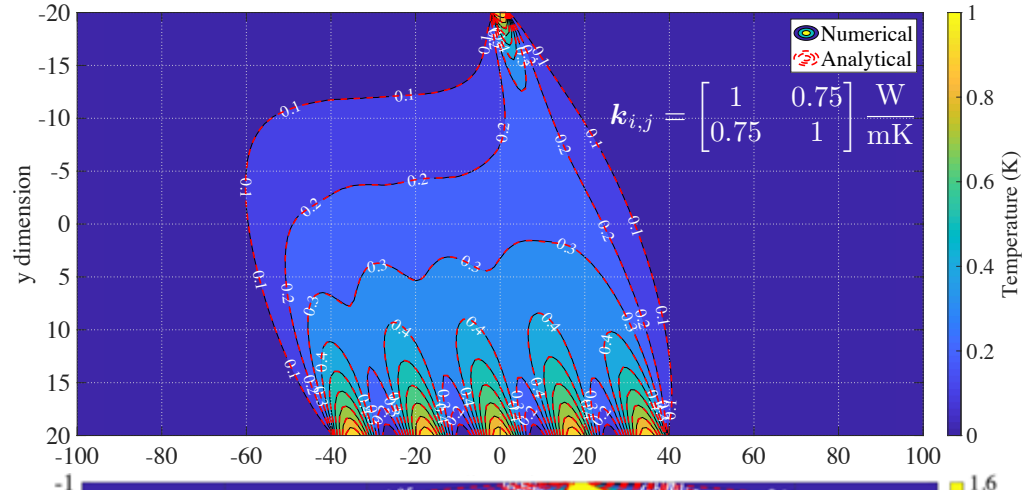


$$\nabla \cdot q = 0 \rightarrow q(x, t) = E(x) T^N(x, t)$$

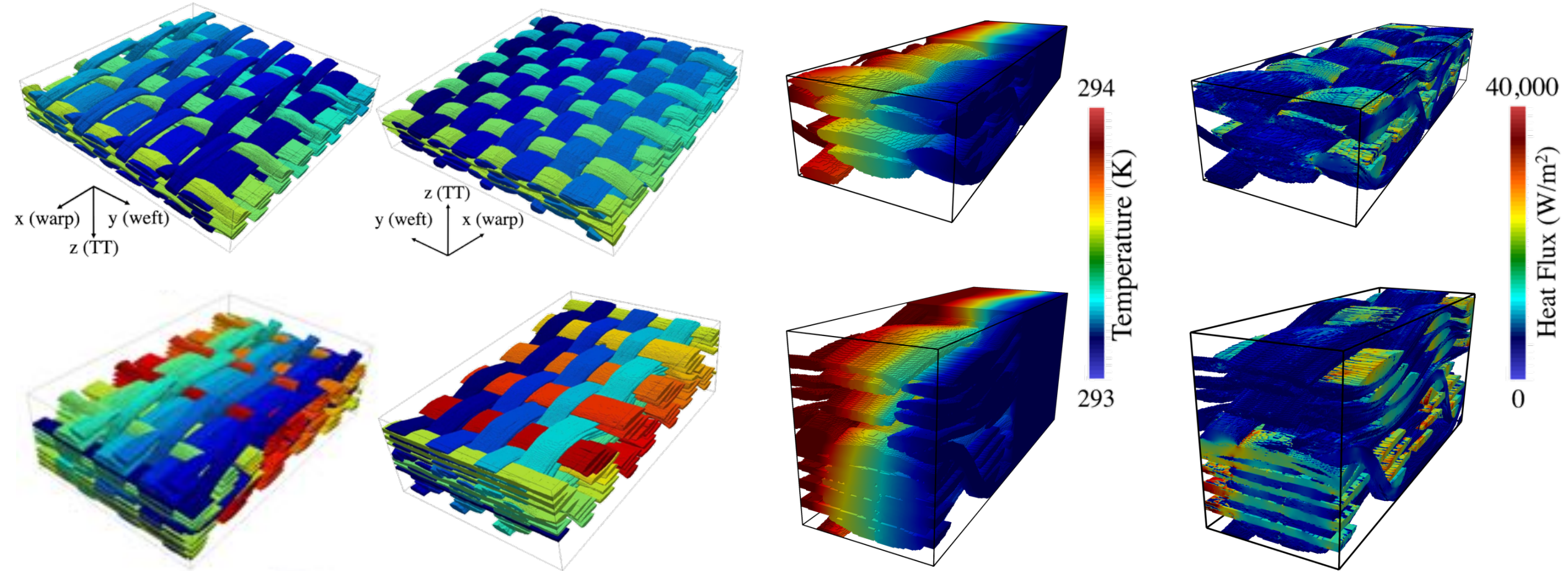
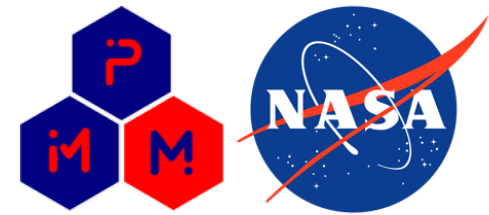
Multi-Point Flux Approximation (MPFA):



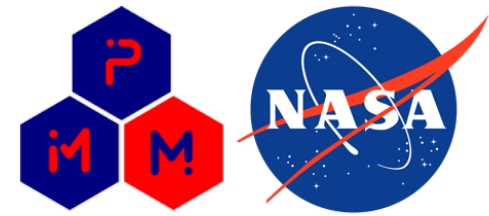
Verification against analytical solutions



ADEPT Validation

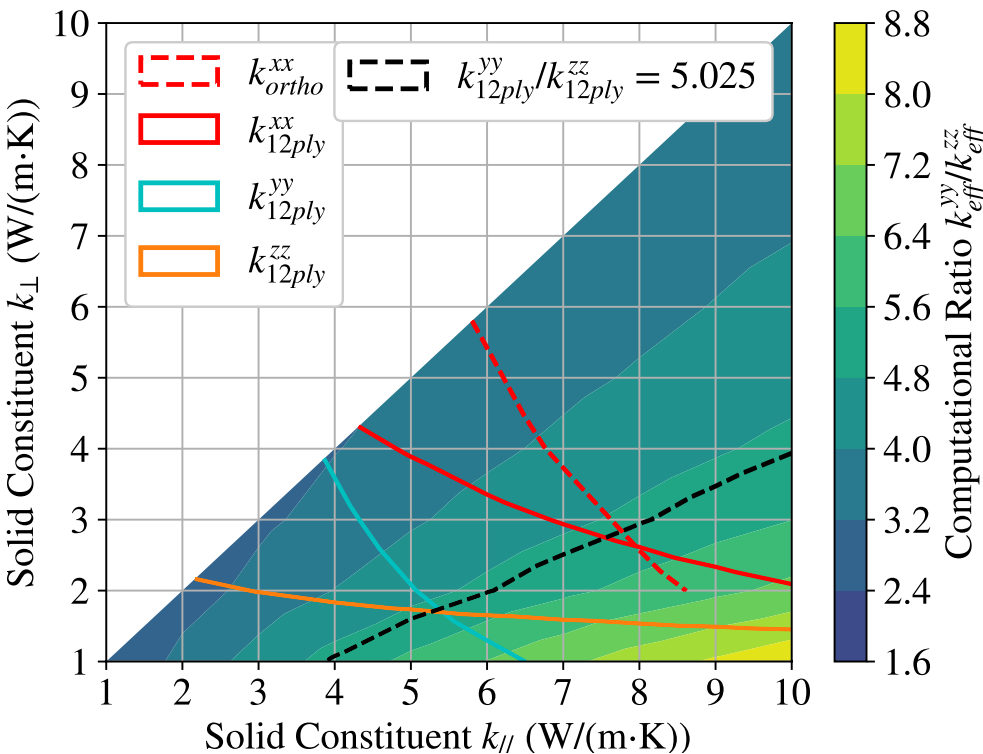


Single Fiber Conductivity Estimation

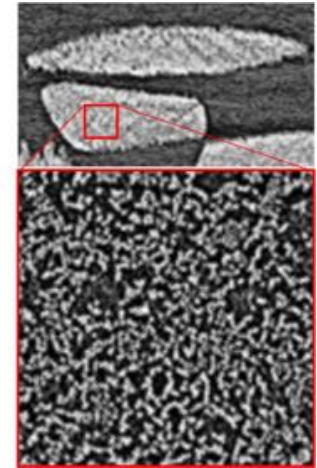
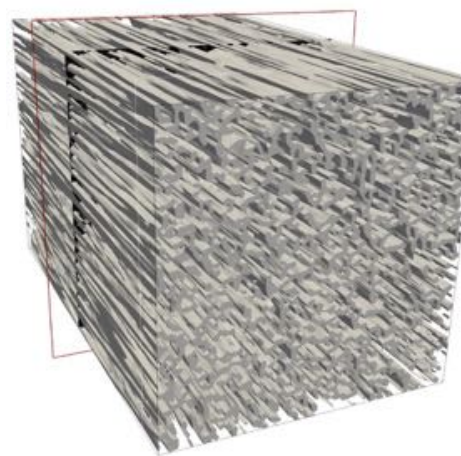


Two experimental values at Room Temperature:

$$\mathbf{k}_{eff}^{ortho} = \begin{bmatrix} 2.342 & - & - \\ - & 1.766 & - \\ - & - & 0.305 \end{bmatrix} \quad \mathbf{k}_{eff}^{12ply} = \begin{bmatrix} 2.184 & - & - \\ - & 1.980 & - \\ - & - & 0.394 \end{bmatrix}$$



$$[k_{//}^{weft}, k_{\perp}^{weft}] = [5.4, 1.8] \quad \text{and} \quad [k_{//}^{warp}, k_{\perp}^{warp}] = [7.7, 2.7] \frac{\text{W}}{\text{mK}}$$



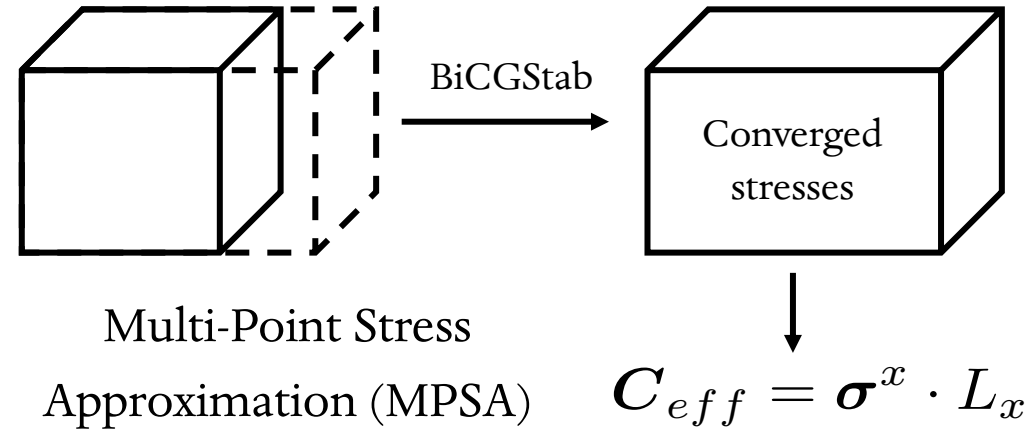
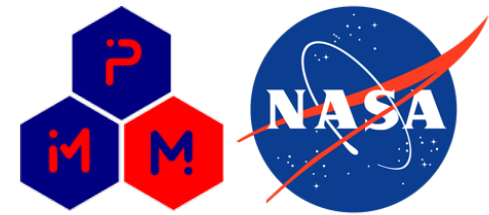
$$[k_{//}, k_{\perp}] = [9.7, 5.5] \frac{\text{W}}{\text{mK}}$$

$$\mathbf{k}_{eff}^{4ply} = \begin{bmatrix} 1.750 & -0.032 & -0.024 \\ -0.093 & 1.490 & 0.002 \\ 0.039 & 0.001 & 0.193 \end{bmatrix} \quad \mathbf{k}_{eff}^{6ply} = \begin{bmatrix} 1.740 & -0.141 & -0.020 \\ -0.105 & 1.710 & -0.005 \\ 0.091 & -0.023 & 0.200 \end{bmatrix}$$

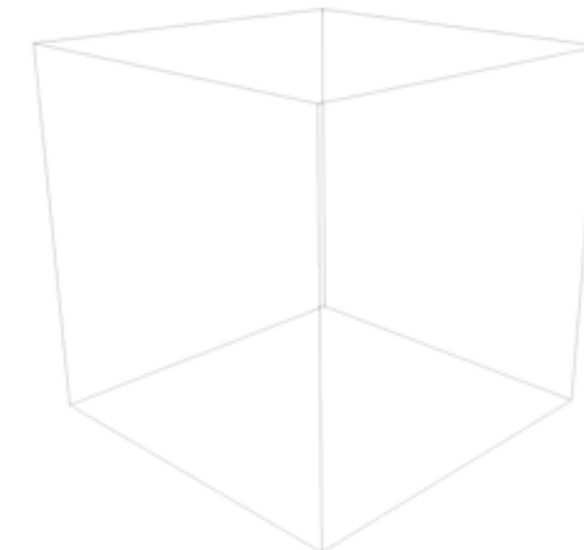
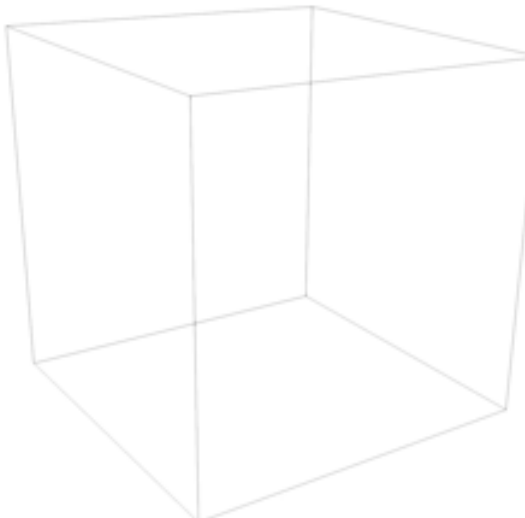
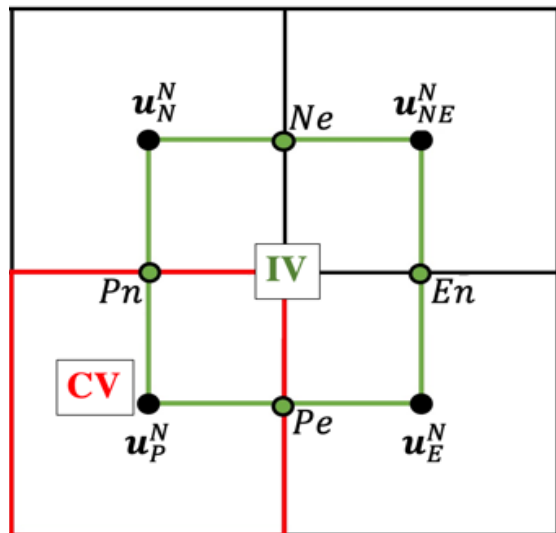
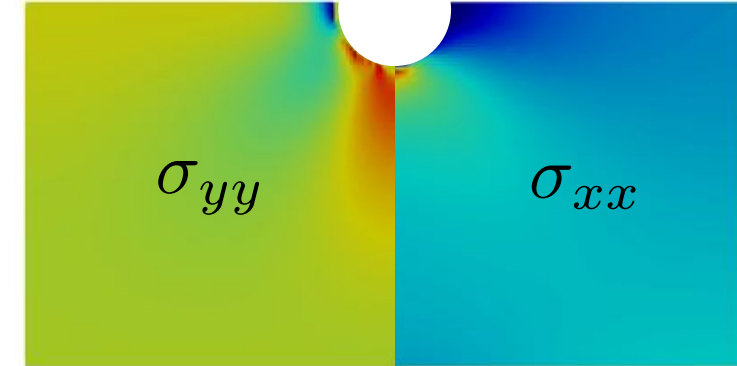
$$\mathbf{k}_{eff}^{8ply} = \begin{bmatrix} 1.830 & -0.244 & 0.016 \\ -0.192 & 1.510 & 0.005 \\ 0.039 & 0.000 & 0.231 \end{bmatrix} \quad \mathbf{k}_{eff}^{12ply} = \begin{bmatrix} 2.310 & -0.414 & 0.000 \\ -0.524 & 2.030 & 0.071 \\ 0.007 & 0.005 & 0.504 \end{bmatrix}^{12}$$

Effective Elasticity

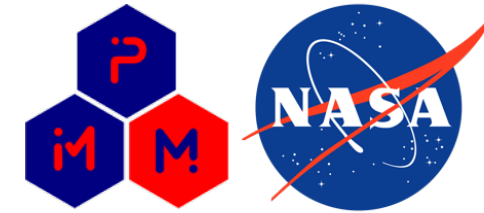
Semeraro, F., Acin, M., Panerai, and Mansour, N.N., Anisotropic analysis of fibrous and woven materials
part 3: Computation of effective elasticity. *Computational Materials Science*, (work in progress)



Verification against analytical solution

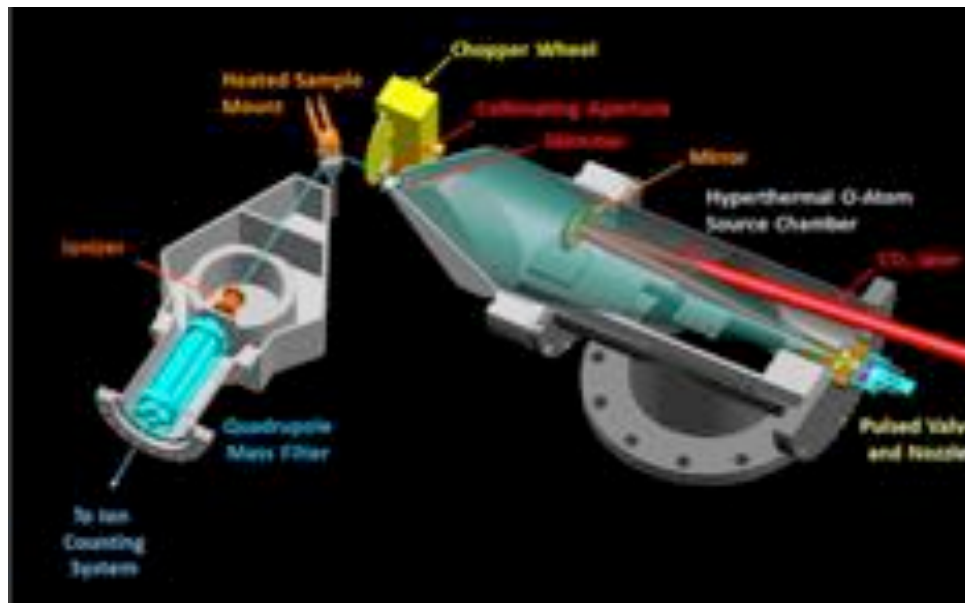


Application motivation

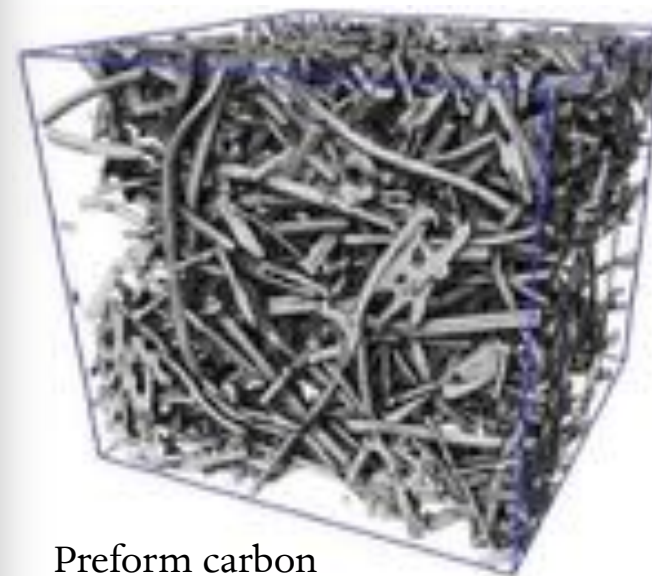


Objectives:

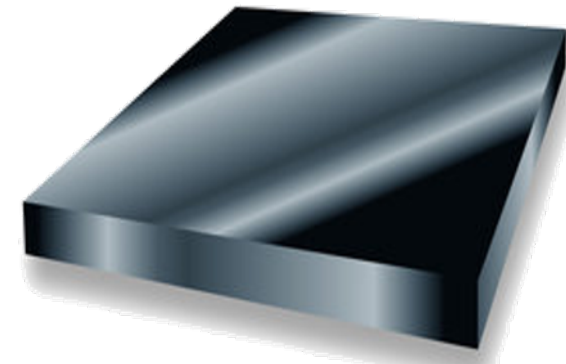
- Characterize recession/ablation of carbon surface coated with NuSil due to oxidation
- Develop a predictive model for use in microscopic (DSMC, PuMA) and macroscopic (CFD, MRC) solvers



Murray *et al*



Preform carbon

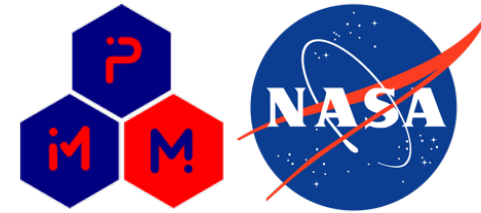


Vitreous carbon

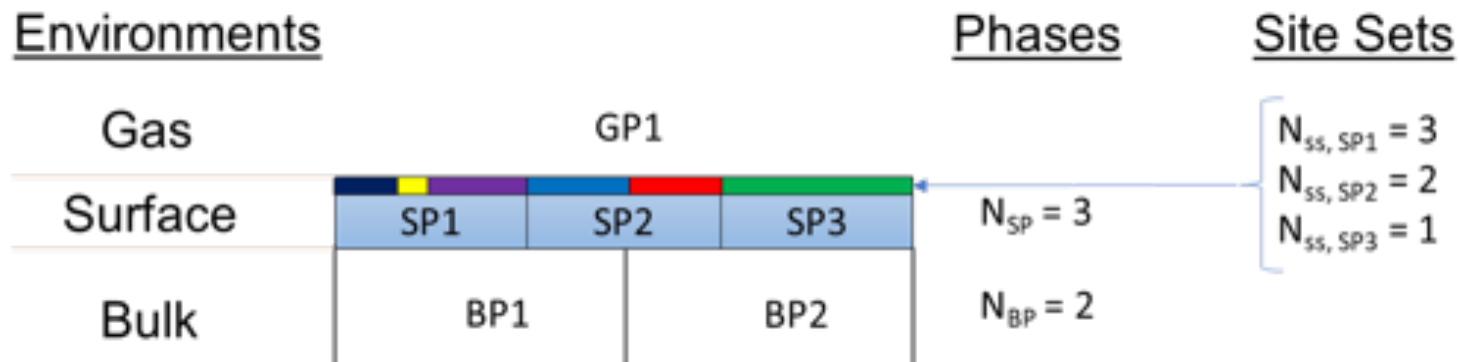
Image courtesy: Prof. Panerai

SPI Supplies

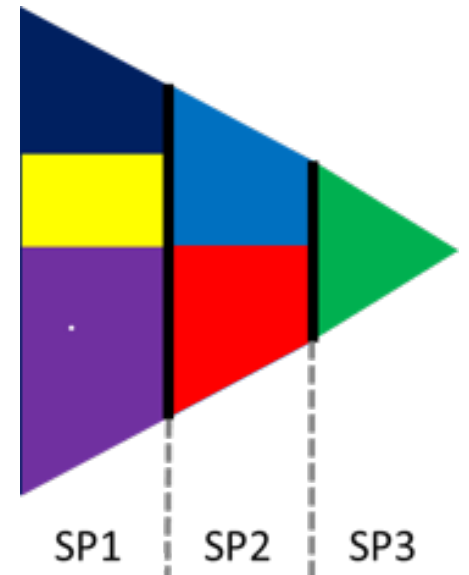
Surface chemistry framework



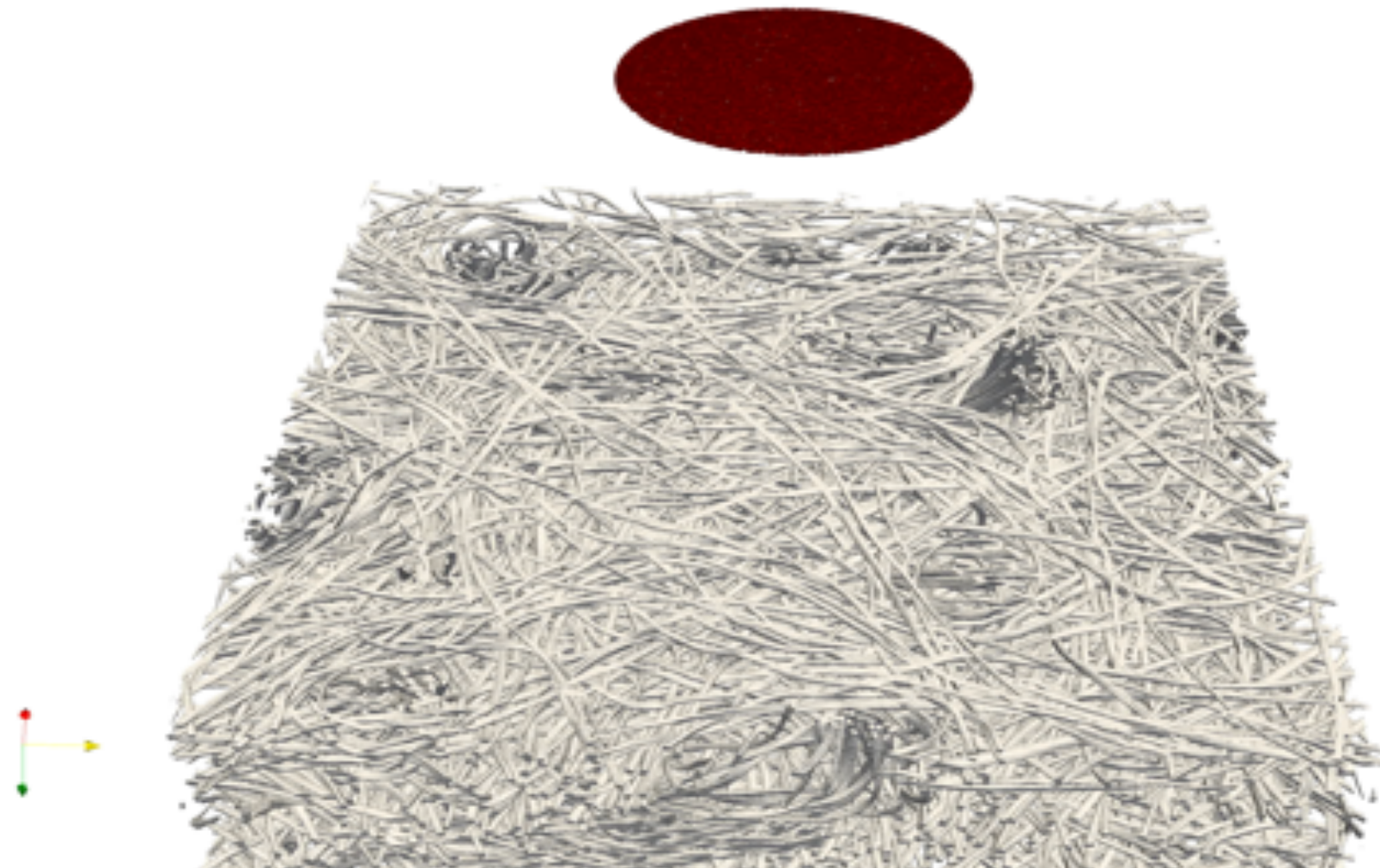
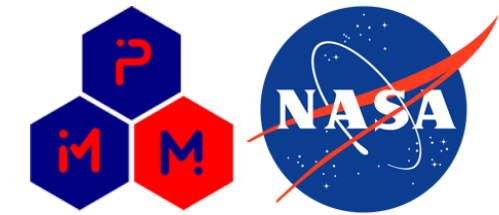
- Methodology to represent surface sites similar to Marschall, Maclean and Driver [4] for CFD.
- Particles adsorbed (deleted) and desorbed (created), surface element stores adsorbed particle concentration.
- Surface reactions based on concentration within surface element.
- Multiple triangulated elements (like cells) on surfaces
- Langmuir model for surface sites.



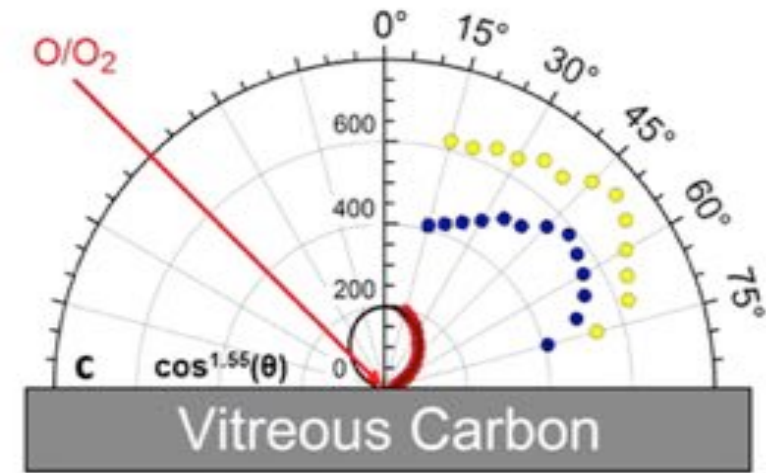
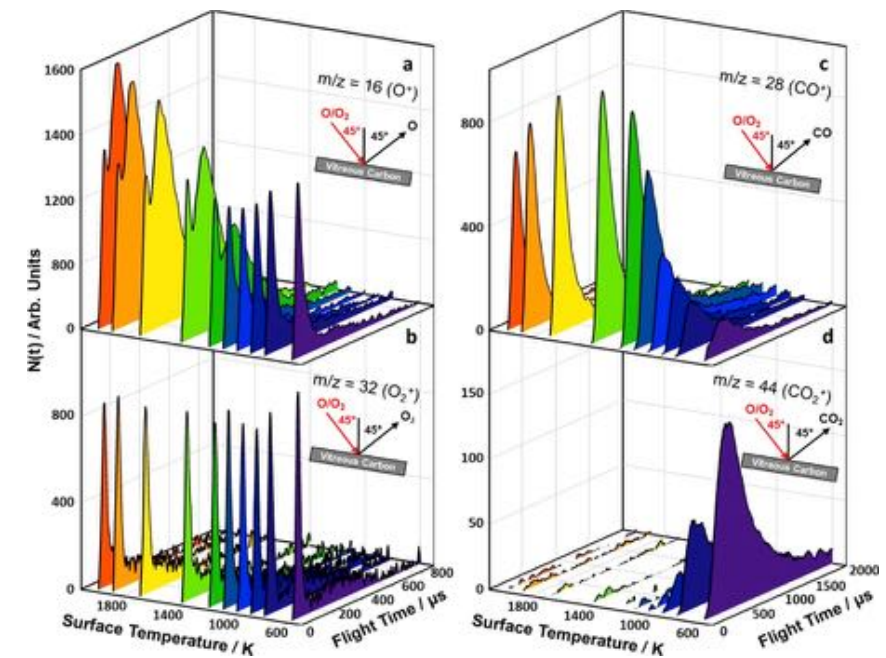
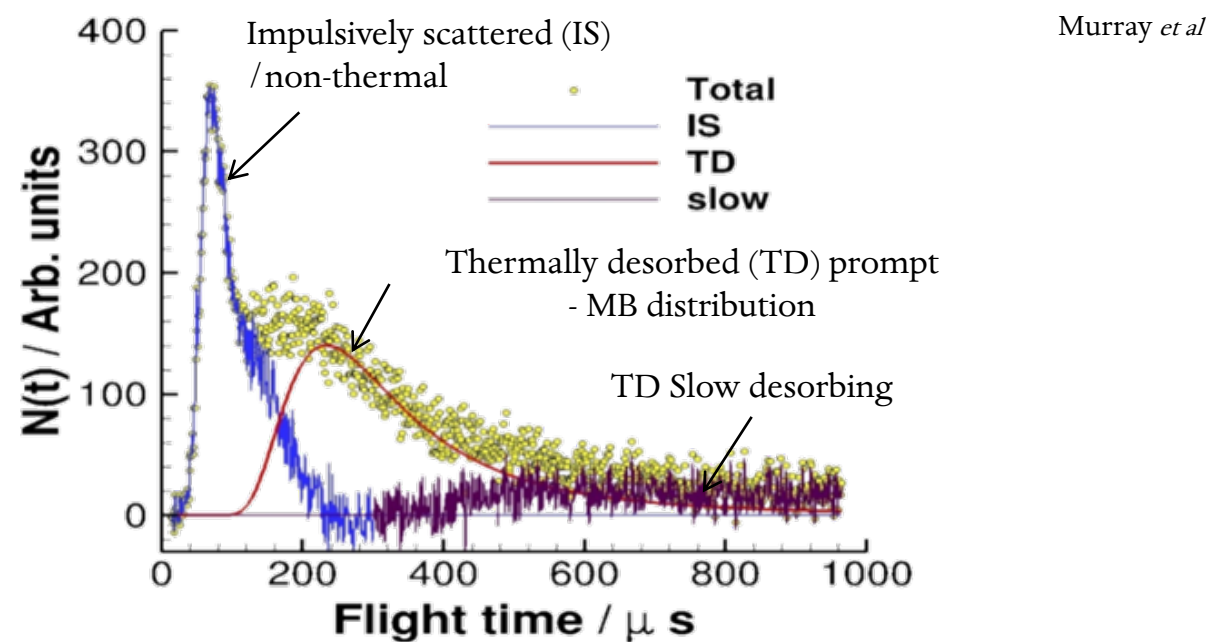
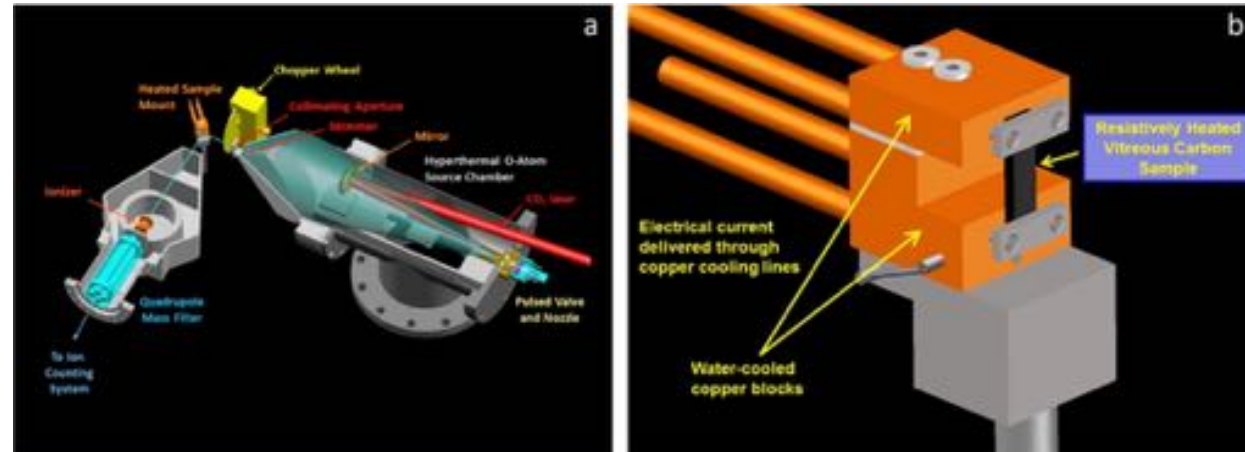
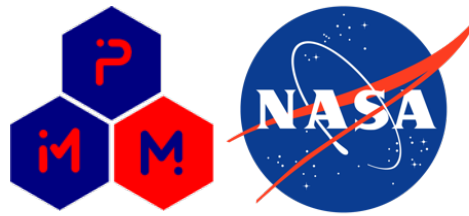
taken from Marschall and Maclean.



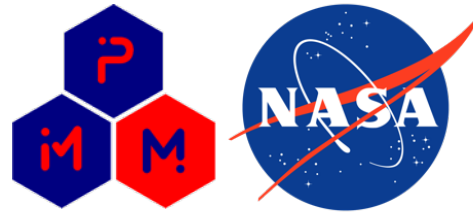
PuMA simulation



Molecular Beam Experimental Setup



Carbon Oxidation Model



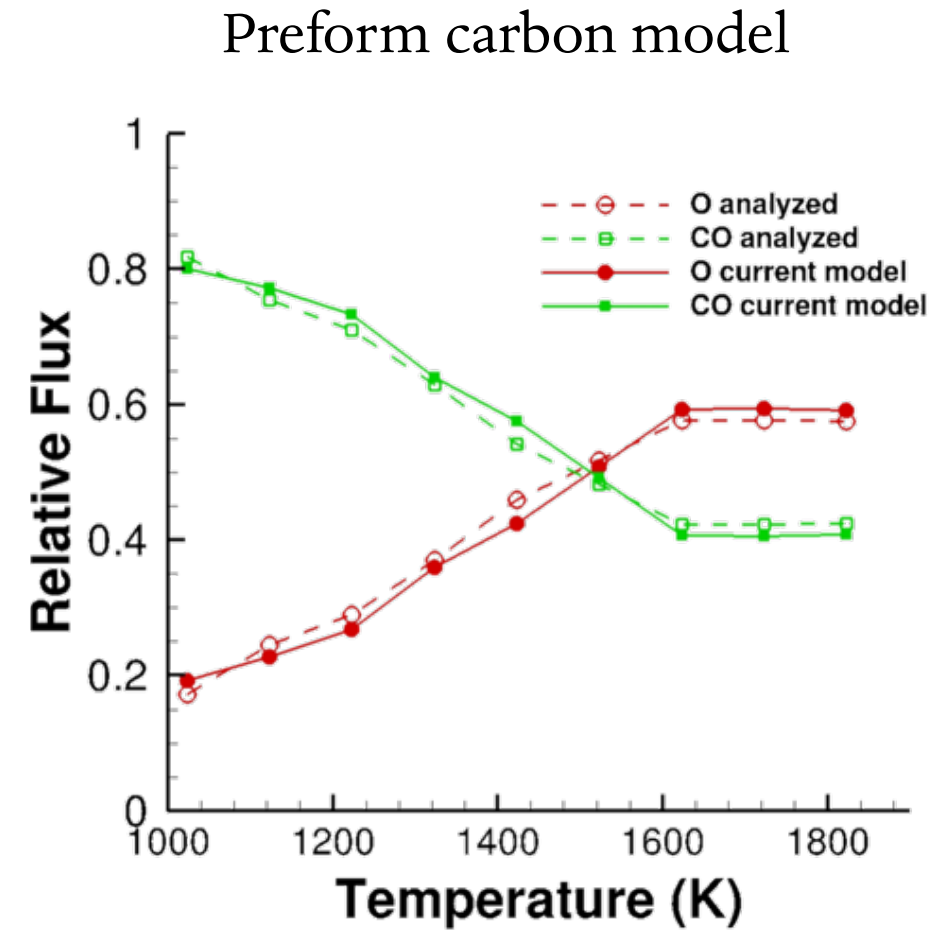
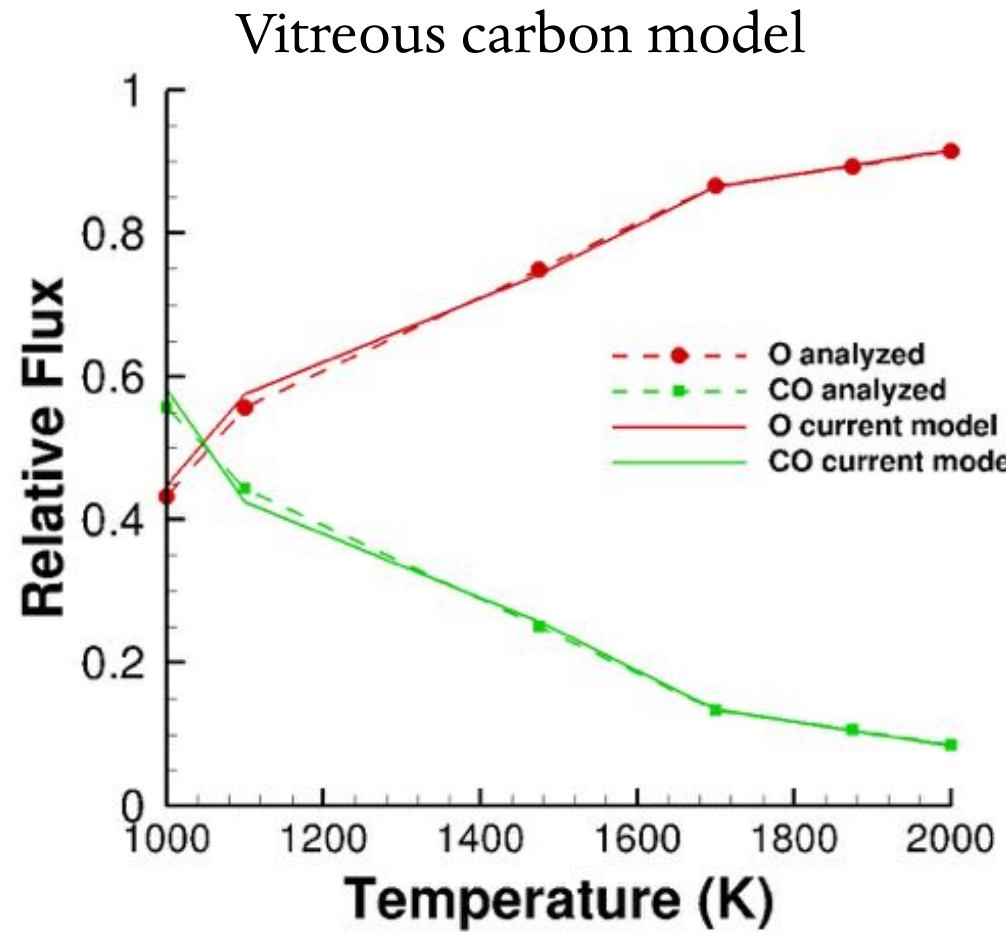
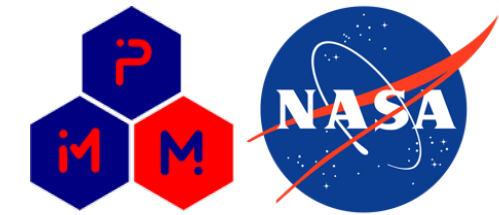
Type	Mechanisms	Reaction
Adsorption	Adsorption	$O(g) + (s) \rightarrow O(ads)$
Adsorption-mediated	LH1 O formation	$O(ads) \rightarrow O(TD)(g) + (s)$
	LH1 CO formation	$O(ads) + C(b) + O'(ads) \rightarrow CO(g) + (s) + O'(ads)$
	LH1 CO ₂ formation	$O(ads) + O(s) + C(b) + 4O'(ads) \rightarrow CO_2(g) + 2(s) + 4O'(ads)$
GS reactions	LH3 O{a} formation	$O(ads) \rightarrow O(a)(s)$
	LH3 CO{a} formation	$O(ads) + C(b) + O'(ads) \rightarrow CO(a)(s) + O'(ads)$
	LH3 CO{b} formation	$O(ads) + C(b) + O'(ads) \rightarrow CO(b)(s) + O'(ads)$
PS reactions	LH3 O{a} desorption	$O(a)(s) \rightarrow O(g) + (s)$
	LH3 CO{a} desorption	$CO(a)(s) \rightarrow CO(g) + (s)$
	LH3 CO{b} desorption	$CO(b)(s) \rightarrow CO(g) + (s)$

Fast TD reactions

Slow formation reactions

Desorption reactions

Vitreous and Preform Carbon model



Effective model for macroscopic solvers

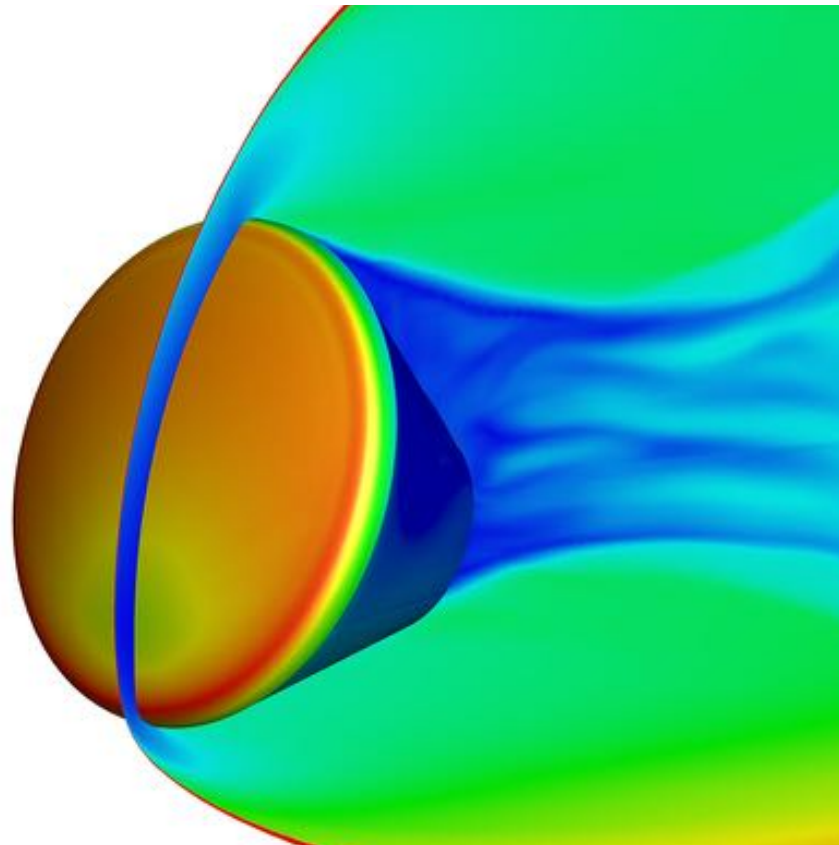
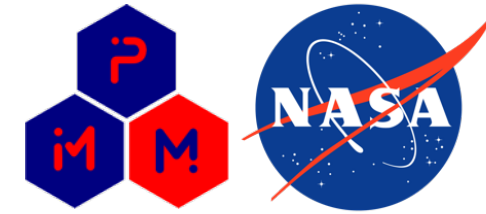
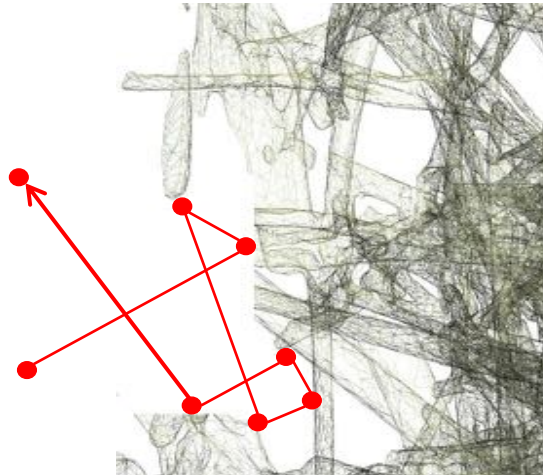
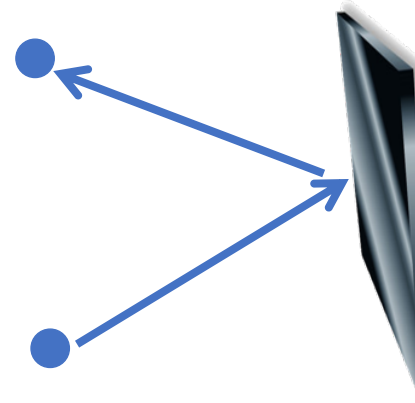


Image credit: NASA

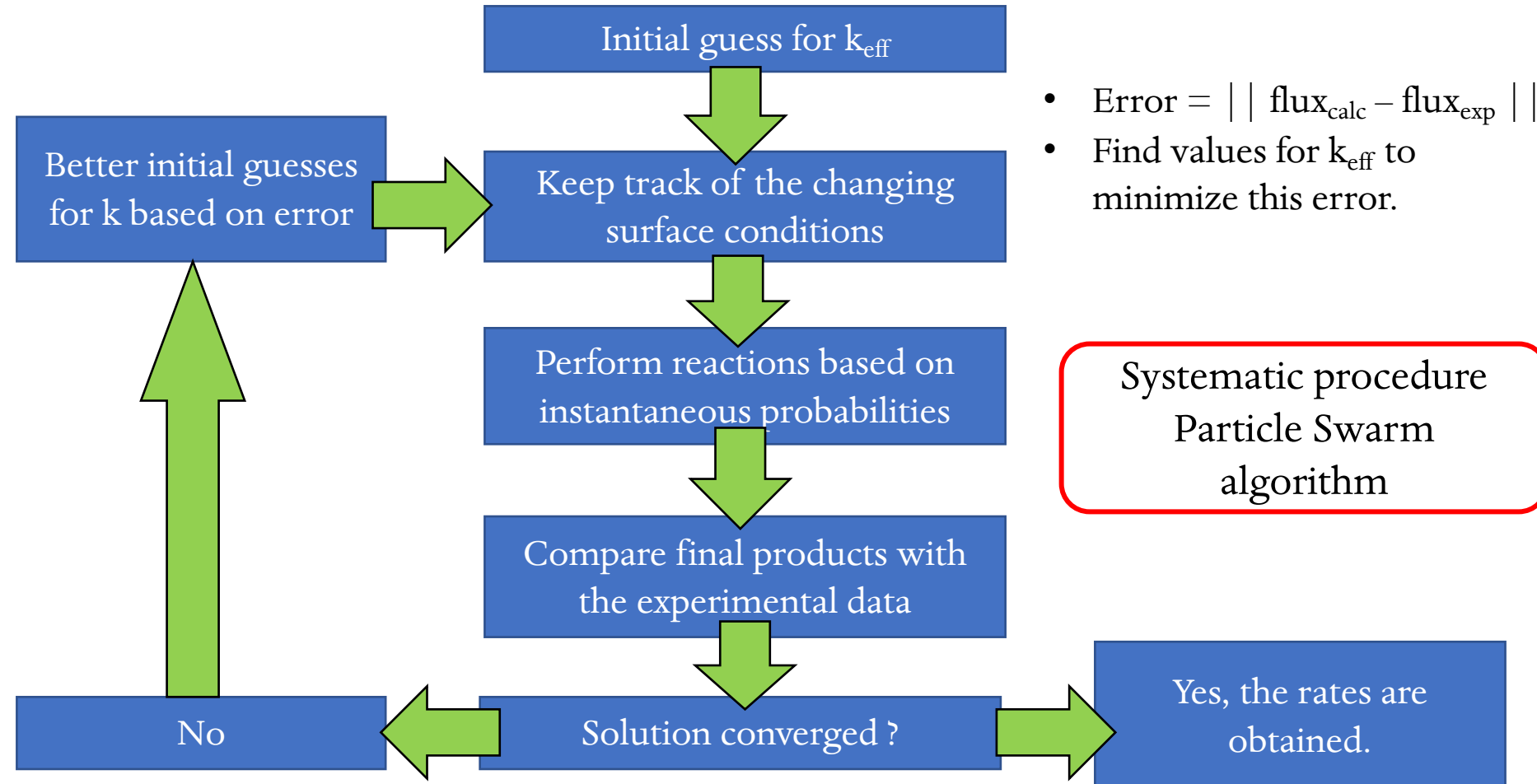
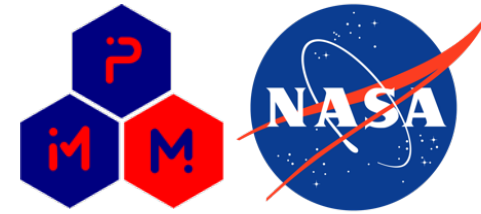


Real model
Rates $\rightarrow k$

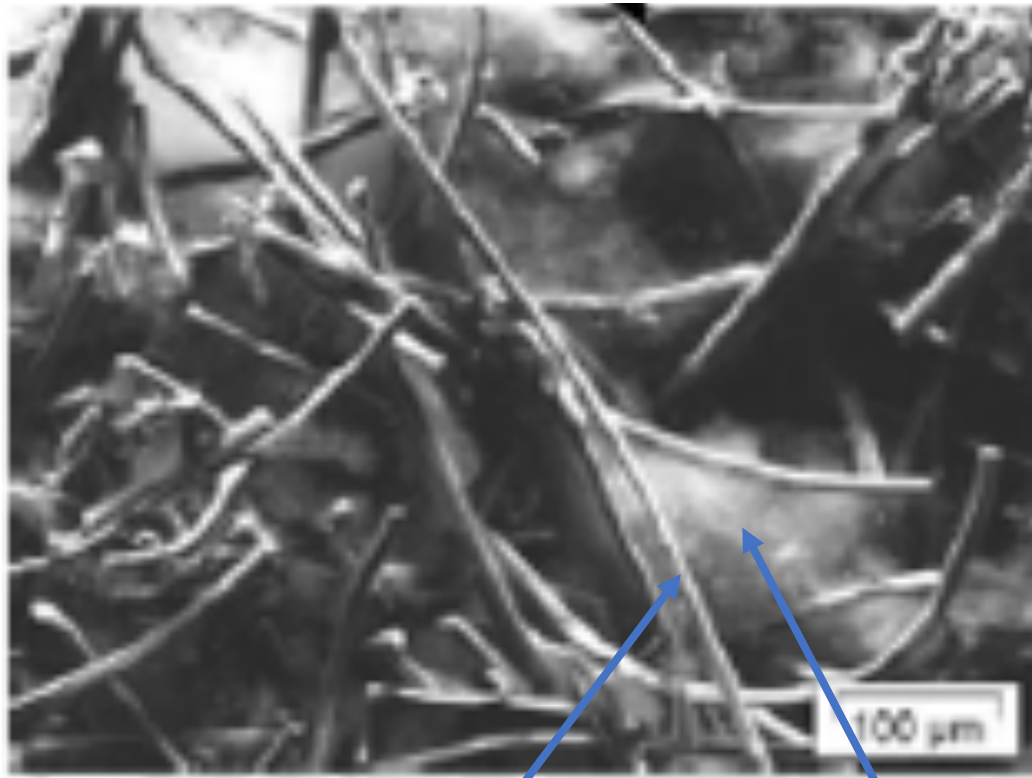
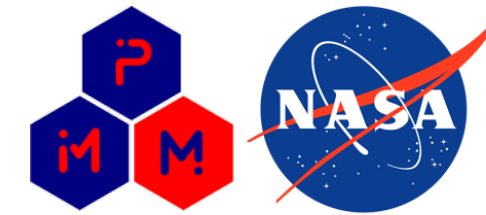


Effective model
Rates $\rightarrow k_{\text{eff}}$

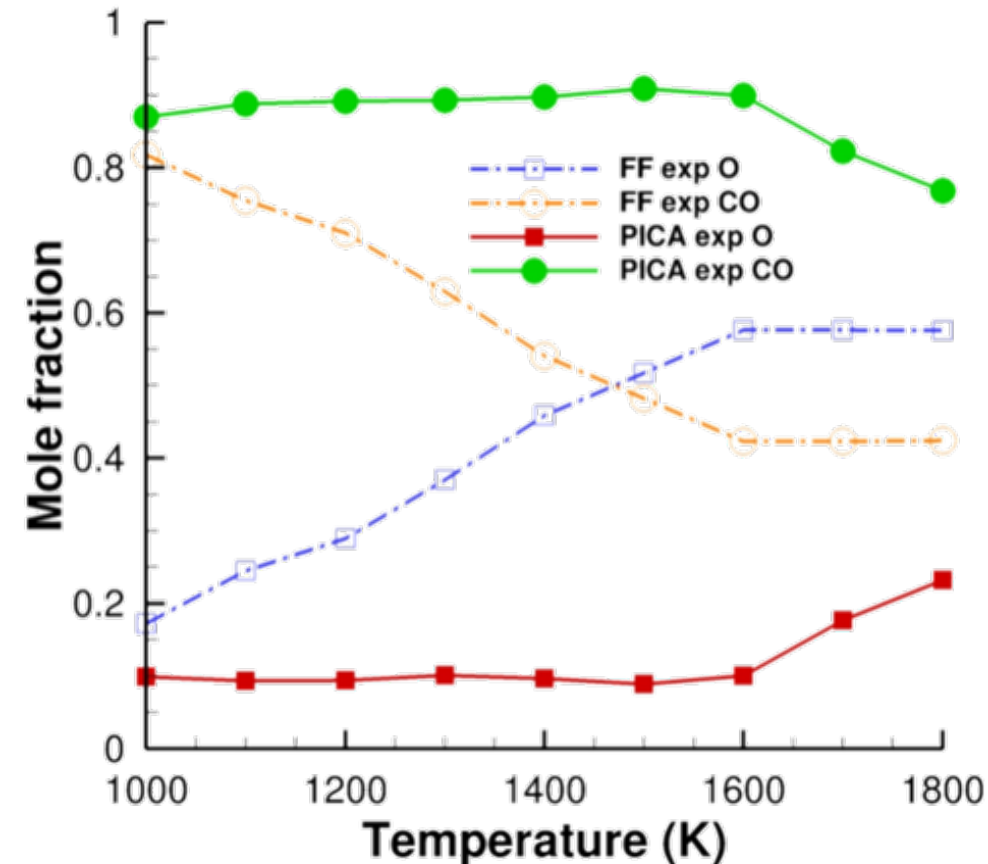
Reaction Rate Constants Fitting Method



PICA oxidation model

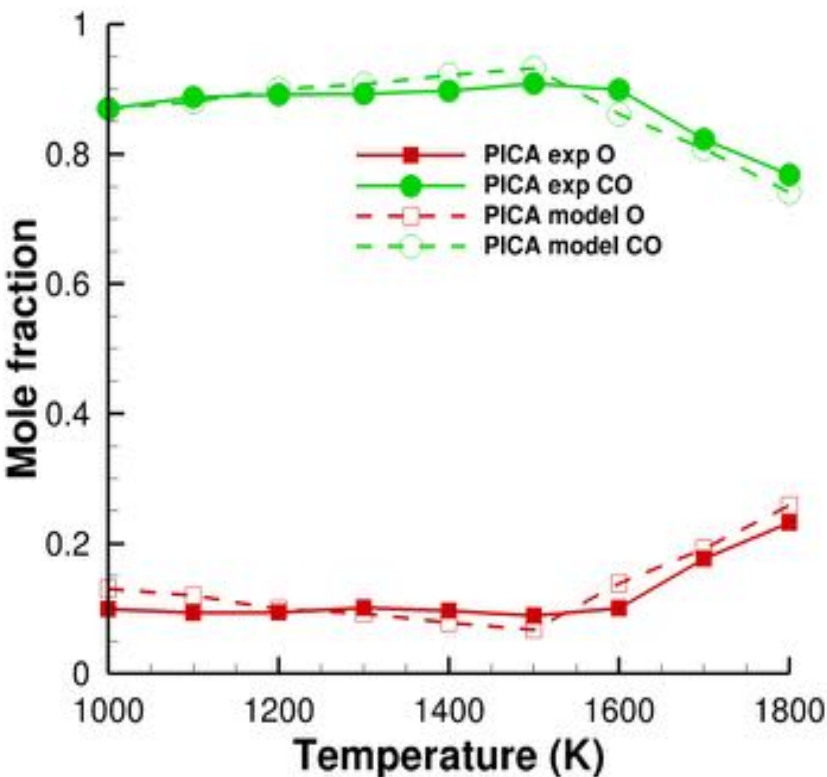
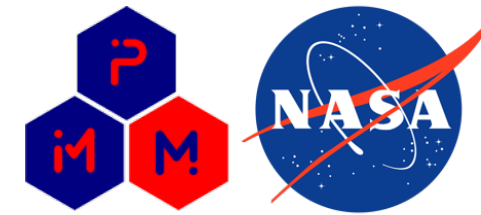


Preform carbon
PICA CHAR
2 phase model



- PICA and FF trends are qualitatively and quantitatively different.
 - Difference in reactivity.
 - Difference in porosity.

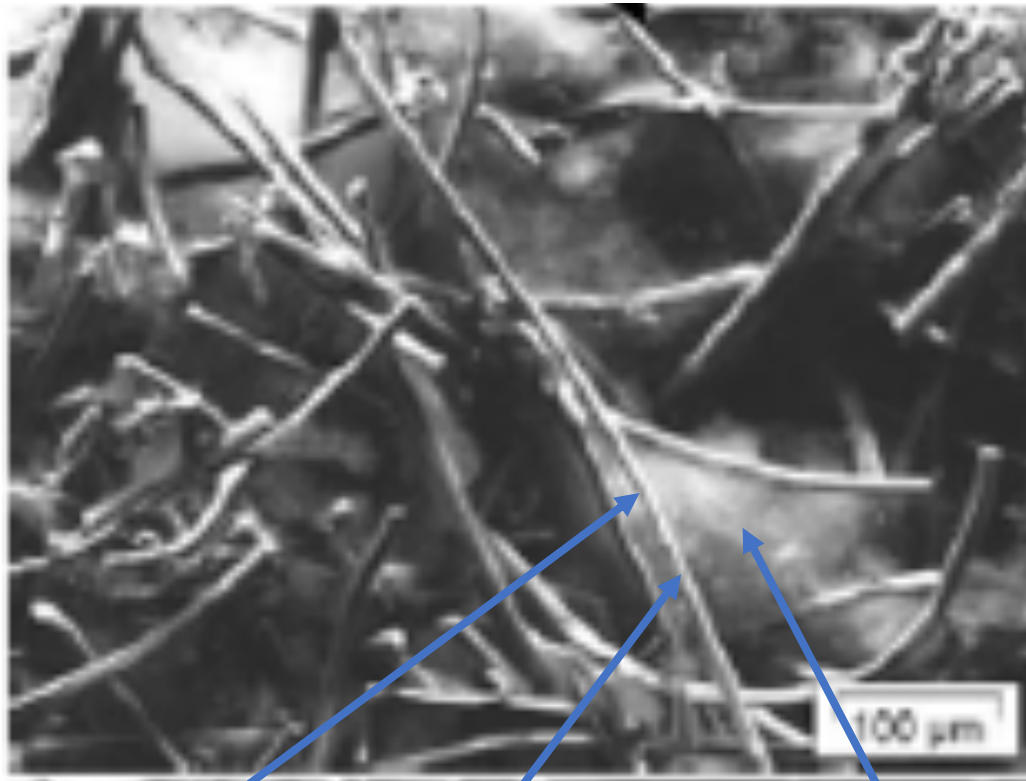
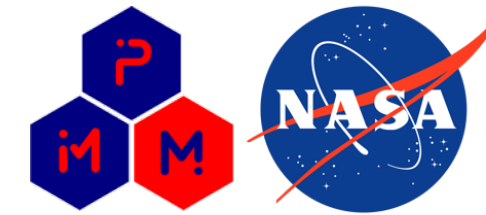
PICA oxidation model



Mechanisms	Reaction	Rate constant (k)
Adsorption	$O(g) + (s) \rightarrow O(ads)$	$\frac{1}{\theta} * \frac{1}{4} \sqrt{\frac{8k_b T_e}{\pi m}} + 1$
TD O formation	$O(ads) \rightarrow O(TD)(g) + (s)$	$0.946 \exp(-\frac{4696.98}{T_e})$
TD CO formation	$O(ads) + C(b) + O'(ads) \rightarrow CO(g) + (s) + O'(ads)$	$\frac{1}{\theta} * 4262.96 \exp(-\frac{7669.41}{T_e})$
LH O[a] formation	$O(ads) \rightarrow O[a](s)$	1
LH CO[a] formation	$O(ads) + C(b) + O'(ads) \rightarrow CO[a](s) + O'(ads)$	$\frac{1}{\theta} * 1226.66 \exp(-\frac{5992.25}{T_e})$
LH CO[b] formation	$O(ads) + C(b) + O'(ads) \rightarrow CO[b](s) + O'(ads)$	$\frac{1}{\theta} * 388.87 \exp(-\frac{2174.87}{T_e})$
LH O[a] desorption	$O[a](s) \rightarrow O(g) + (s)$	$0.05 T^2 \exp\left(-\frac{3177.2}{T_e}\right)$
LH CO[a] desorption	$CO[a](s) \rightarrow CO(g) + (s)$	$4485.5 \exp\left(-\frac{1581.4}{T_e}\right)$
LH CO[b] desorption	$CO[b](s) \rightarrow CO(g) + (s)$	$1.20 \exp\left(-\frac{3251.60}{T_e}\right)$

- New 2 phase model for PICA
 - Phase 1: FiberForm – same rates as preform carbon model.
 - Phase 2: PICA char – new rates for same reactions.
- Newly developed PICA model agrees well with the experiments.

PICA-NuSil oxidation model

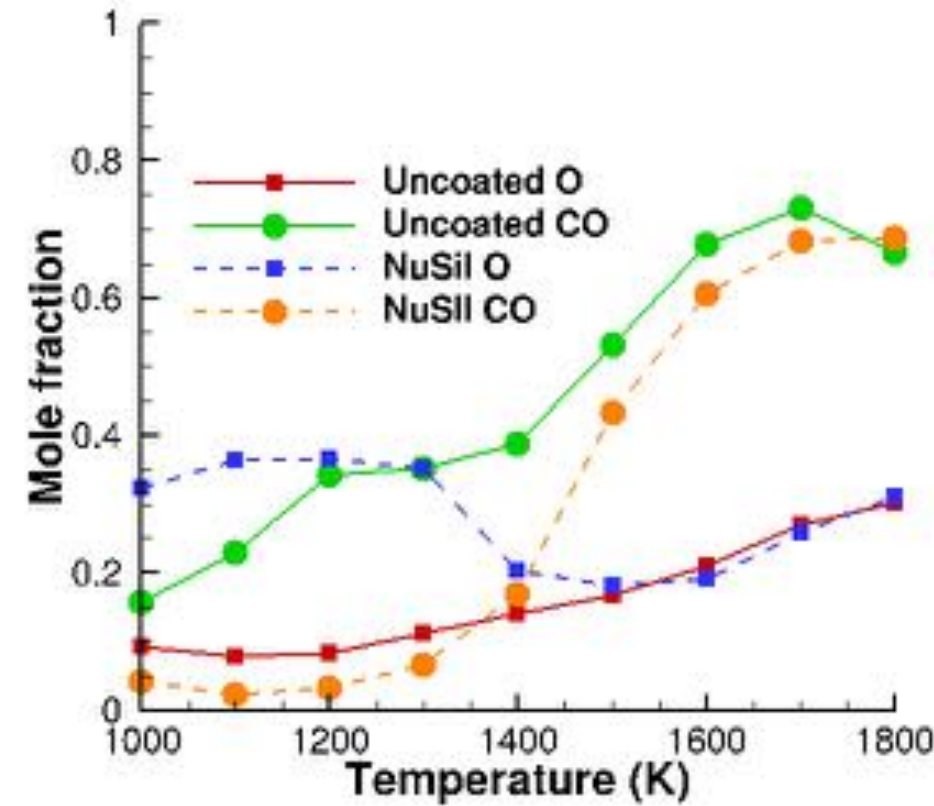


NuSil

Preform carbon

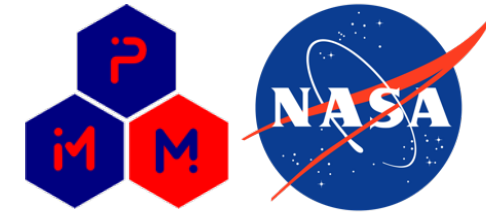
PICA
CHAR

3 phase model

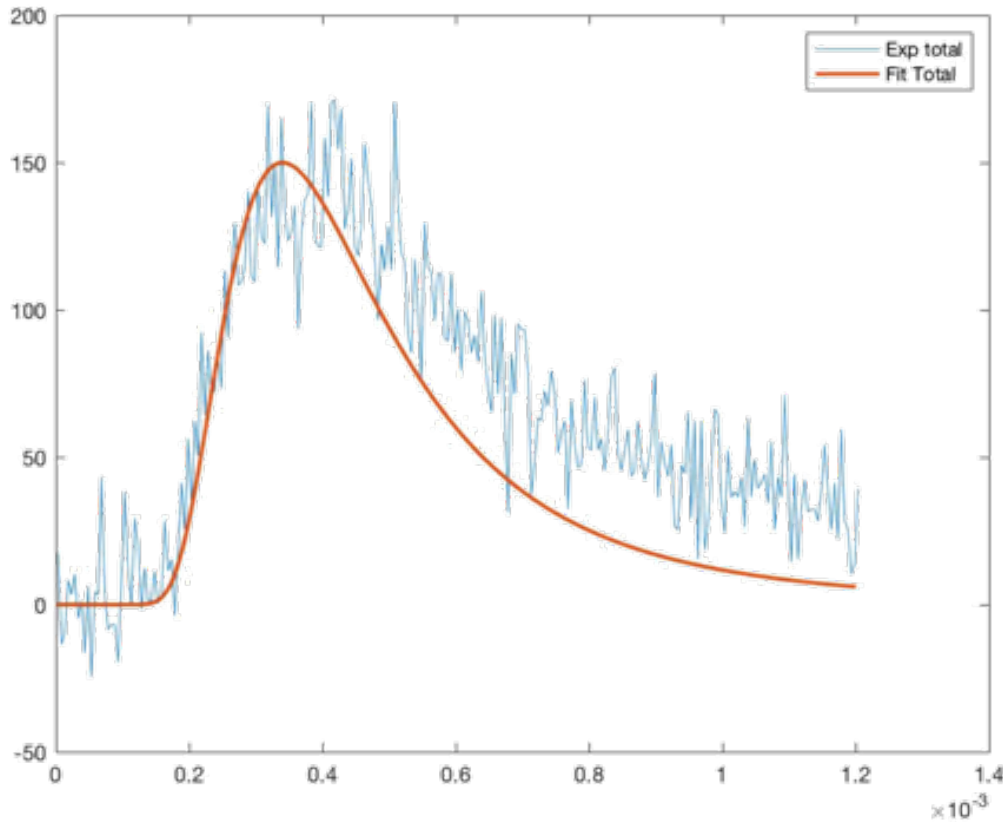


- PICA and FF trends are qualitatively and quantitatively different.
 - Difference in reactivity.
 - Difference in porosity.

SiO reactions



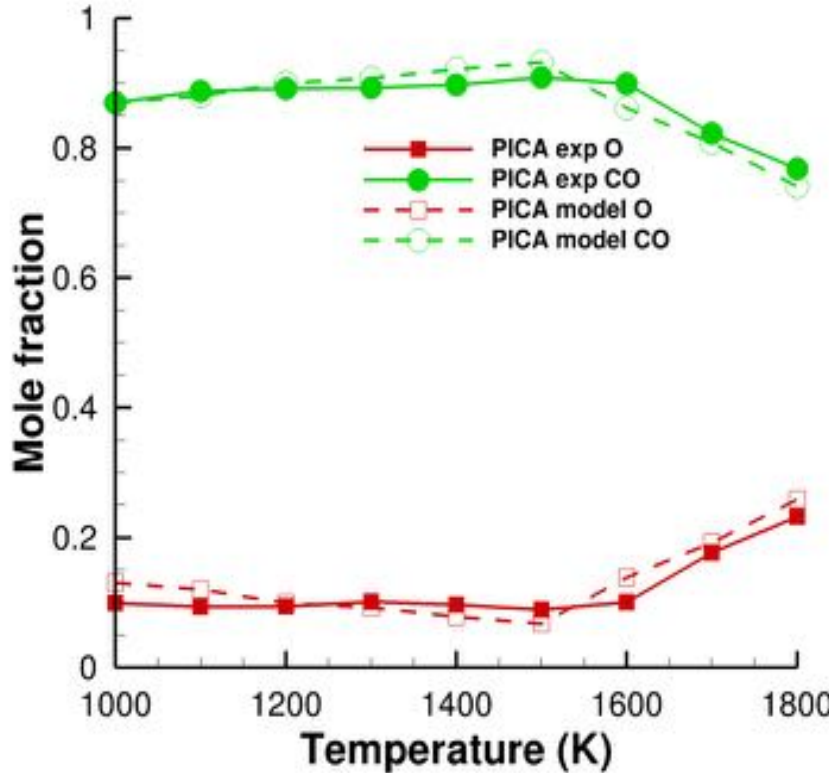
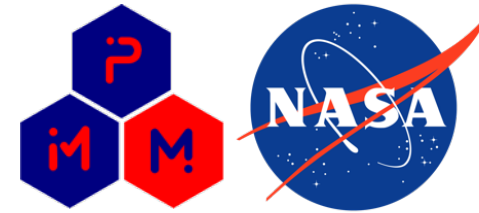
PICA-NuSil T = 1800K SiO TOF



Mechanisms	Reaction
Scattering	$O(g) + Si(s) \rightarrow O(g) + Si(s)$
TD SiO formation	$O(g) + Si(s) \rightarrow SiO(g) + (s)$
LH SiO formation	$O(g) + Si(s) \rightarrow SiO(g) + (s)$

- SiO TOF has a fast TD and slow desorption component.

PICA-NuSil oxidation model



Mechanisms	Reaction
Scattering	$O(g) + Si(s) \rightarrow O(g) + Si(s)$
TD SiO formation	$O(g) + Si(s) \rightarrow SiO(g) + (s)$
LH SiO formation	$O(g) + Si(s) \rightarrow SiO(g) + (s)$

- New 3 phase model for PICA-NuSil
 - Phase 1: FiberForm – same rates as preform carbon model.
 - Phase 2: PICA char – same rates as PICA 2 phase model.
 - Phase 3: NuSil – new rates for same reactions.
- Newly developed PICA-NuSil model agrees well with the experiments.